JOURNAL OF THE AMERICAN CHEMICAL SOCIETY

Communication

pubs.acs.org/JACS

TAT Peptide-Functionalized Gold Nanostars: Enhanced Intracellular Delivery and Efficient NIR Photothermal Therapy Using Ultralow Irradiance

Hsiangkuo Yuan,[†] Andrew M. Fales,[†] and Tuan Vo-Dinh*[,†,‡,§]

[†]Department of Biomedical Engineering, [‡]Department of Chemistry, and [§]Fitzpatrick Institute for Photonics, Duke University, Durham, North Carolina 27708, United States

Supporting Information

ABSTRACT: Gold nanoparticles have great potential in plasmonic photothermal therapy (photothermolysis), but their intracellular delivery and photothermolysis efficiency have yet to be optimized. We show that TAT-peptide-functionalized gold nanostars (NS) enter cells significantly more than bare or PEGylated NS. The cellular uptake mechanism involves actin-driven lipid raft-mediated macropinocytosis, where particles primarily accumulate in macropinosomes but may also leak out into the cytoplasm. After 4-h incubation of TAT-NS on BT549 breast cancer cells, photothermolysis was accomplished using 850 nm pulsed laser under 0.2 W/cm^2 irradiation, below the maximal permissible exposure of skin. These results demonstrate the enhanced intracellular delivery and efficient photothermolysis of TAT-NS, promising agents in cancer therapy.

Nanoparticle (NP) systems have gained wide attention due to their potential in medicine, e.g., molecular imaging, immunization, theranostics, and targeted delivery/therapy.[1] NP can be fabricated as strong contrast agents for different imaging modalities with better signal-to-noise ratios than conventional agents,[2a] or as therapeutic agents such as drug carriers,[2b] radioenhancers,[2c] and photothermal transducers.[2d] Gold nanoparticles (AuNP), offering facile synthesis and biocompatibility, have been applied for a variety of therapeutics, especially in cancer therapy.[3a,b]

Gold nanostars (AuNS), which feature tunable plasmon bands in the near-infrared (NIR) tissue optical window, have potential for *in vivo* imaging and therapeutic applications.[4a−c] Previously, metal NP imaging has required the use of fluorescent labels, which are generally quenched on the gold surface. Other non-fluorescent optical tracking methods, using dark-field or differential interference contrast, are typically inoperable in tissue samples.[5] AuNS, with their unique plasmon resonating with the NIR incident light, create a nonlinear field enhancement that yields intense two-photon photoluminescence (TPL). Their extremely high two-photon action cross section (e.g., 10^6 GM), which is several orders of magnitude higher than that of organic fluorophores, allows both *in vitro* and *in vivo* real-time NS tracking without the use of fluorescence.[4b,c,6] The ability to visualize NS with high temporal and spatial resolution under multiphoton microscopy provides tremendous flexibility in studying NP kinetics/trafficking behavior in biomedical settings.

Moreover, with a high absorption-to-scattering ratio in the NIR and multiple sharp edges favorable for heat generation, NS efficiently transduce photon energy into heat for hyperthermia therapy.[4c,7] To date, most photothermolysis studies utilize laser irradiation higher than the maximal permissible exposure (MPE) of skin per ANSI regulation.[8] Previously, *in vitro* photothermolysis using NIR pulsed laser reported irradiances of 1.5−48.6 W/cm^2,[6a,9] higher than the MPE of skin (e.g., 0.4 W/cm^2 at 850 nm). Insufficient intracellular particle delivery and low photothermal transduction efficiency may be the main obstacles. Therefore, there is a strong need to design a more efficient photothermal transducer for pulsed lasers (e.g., AuNS) with optimized cellular uptake. Here, we present TAT-peptide-functionalized AuNS for both enhanced intracellular particle delivery and efficient *in vitro* photothermolysis using a NIR femtosecond laser under an irradiance of 0.2 W/cm^2, lower than the MPE of skin.

To achieve successful and selective photothermolysis, NS need to be delivered sufficiently to the designated target cells without compromising cells' viability. In general, NP's size, shape, surface charge, and coating (e.g., protein corona, polymer, antifouling layer) all affect their cellular delivery.[11] People have tried numerous methods to increase the uptake of NP. One of the most efficient ways to do this is achieved by surface coating with cell-penetrating peptides (CPPs).[10a]

CPPs, with 30 or fewer amino acids that are cationic or amphipathic in nature, facilitate translocation across the cellular membrane. Human immunodeficiency virus type 1 (HIV-1)-encoded TAT peptide, one of the most studied CPPs, has been employed to facilitate not only the intracellular delivery of various NP[12a−c] but also the crossing of the blood−brain barrier (BBB).[12d,e] TAT functionalization on NS could therefore enhance intracellular delivery, which in turns allows efficient photothermolysis with lower irradiance. To date, although enhanced cellular uptake of TAT-labeled AuNP (TAT-AuNP) has already been observed,[11a,12a,14] the cellular uptake mechanism remains unreported. We will therefore employ TAT-functionalized nanostars (TAT-NS) as a model system to study their cellular uptake mechanism and temporal profile.

Received: April 30, 2012
Published: June 26, 2012

dx.doi.org/10.1021/ja304180y | *J. Am. Chem. Soc.* 2012, 134, 11358−11361

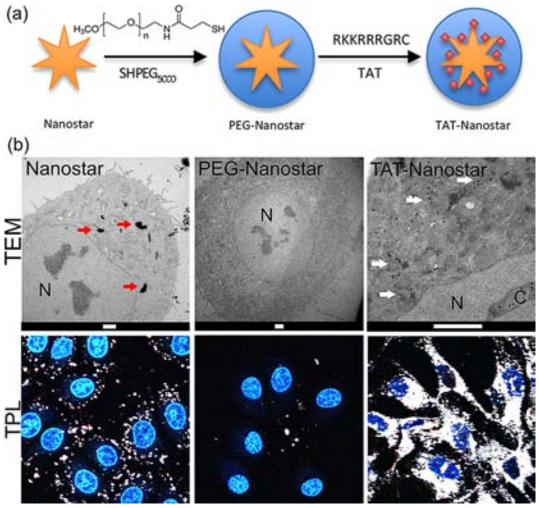

Figure 1. (a) Schematics for TAT coating on gold nanostars. Bare NS was coated with thiolated-PEG to stabilize the NS, then with cysteine-terminated TAT. (b) Cellular uptake of 0.1 nM bare NS, PEG-NS, and TAT-NS incubated 24 h on BT549 cells. Aggregated bare NS (red arrows) in the TEM image correlate to the white big punctates in the TPL image. PEG-NS showed no uptake. Endosomal (white arrows) and cytosolic (black punctates) TAT-NS in the TEM image correlate to the diffuse white pattern in the TPL image. N, nucleus; C, cleft; scale bar, 2 μm; TPL image size, 125×125 μm^2.

TAT-NS were synthesized as illustrated in Figure 1a. To fabricate stable TAT-NS that resist aggregation in physiological environment and multiple washing cycles, cysteine-terminated TAT peptide (cTAT) and thiolated polyethylene glycol (SHPEG) were both used. We noticed that adding cTAT to NS before adding SHPEG leads to early aggregation. A reverse sequence,[5a] adding cTAT into PEGylated NS (PEG-NS), resulted in stable TAT-NS (Figure S1, Supporting Information). The ζ-potential increased from −25.5 (PEG-NS) to −17.6 mV (TAT-NS). Enhanced intracellular delivery of TAT-NS (Figure 1b) further confirms the presence of TAT on NS.

Figure 1b clearly shows enhanced intracellular delivery of TAT-NS, which can be easily visualized under TPL microscopy with high spatial resolution. Cellular uptake of TAT-NS may differ between cell lines.[5b] Here we use the BT549 breast cancer cell line as a model to demonstrate enhanced particle delivery. For the first time, the intracellular distribution of TAT-NS, PEG-NS, and bare NS was investigated with both transmission electron microscopy (TEM) and TPL imaging. In the TEM images, numerous TAT-NS are either clustered in vesicles or scattered in the cytoplasm (Figure S2). This corresponds to the diffuse white pattern seen in the TPL image (Figure 1b). Because the two-photon axial point-spread function for a 20× water objective is ~1.7 μm,[15] each TPL image may constitute an optical thickness of >20 ultratome thin sections (~70 nm). For example, 100 NS seen in a TEM image correlates to ~2000 NS in a TPL image. This could explain why TAT-NS are nearly "saturated" inside cells in the TPL image. Meanwhile, TAT-NS were observed in the nuclear region on TPL imaging. However, upon examining several cells by TEM, we did not find any true intranuclear TAT-NS, except some particles in the nuclear cleft, which still appeared to be in the cytoplasm. This agrees with recent studies showing intranuclear localization of smaller TAT-functionalized NP of 50 nm or less.[14a,b,16] The mismatch between TPL and TEM images suggests that intracellular particle distribution characterization using optical methods should be confirmed by TEM. In agreement with previous studies,[3b,11a] PEGylation resulted in only minimal cellular uptake at this particle concentration. Bare NS without a protective layer tend to aggregate in the vesicles, forming large dense spots in the TEM image, corresponding to big white punctates in the TPL image. Comparing these surface modifications (TAT, PEG, bare), TAT functionalization greatly facilitates the uptake of AuNS.

TAT peptide operates by anchoring on the plasma membrane and translocating primarily via macropinocytosis, i.e., formation of large endocytic vesicles of irregular sizes and shapes, generated by actin-driven invagination of the plasma membrane.[10b] It has been shown that TAT peptide, through multidentate hydrogen bonding of arginines (not lysines) with the anionic groups on the membrane (e.g., heparan sulfate proteoglycans, filamentous actin), causes membrane deformation and cytoskeleton reorganization (e.g., actin ruffling) to translocate either directly through the membrane or via endocytosis.[17] TAT-functionalized proteins or QD also enter cells via macropinocytosis;[13] however, this process has yet to be properly characterized on TAT-AuNP. We therefore applied both TEM and TPL imaging to assess the TAT-NS intracellular trafficking pathway.

The TEM images in Figure 2b show numerous TAT-NS bound to the membrane. The binding was not homogeneous throughout the membrane but formed a patchy distribution, possibly as a result of heterogeneous distribution of heparan sulfate proteoglycans associated with lipid rafts. Figure 2b also shows the surface ruffling in the process of forming a large macropinosome to take up TAT-NS. The ruffling is a common behavior in macropinocytosis.[10b] In addition, the vesicle sizes in Figure 2b are ~500 nm, larger than typical vesicle size for clathrin- (100−150 nm) or caveola-mediated (50−60 nm)

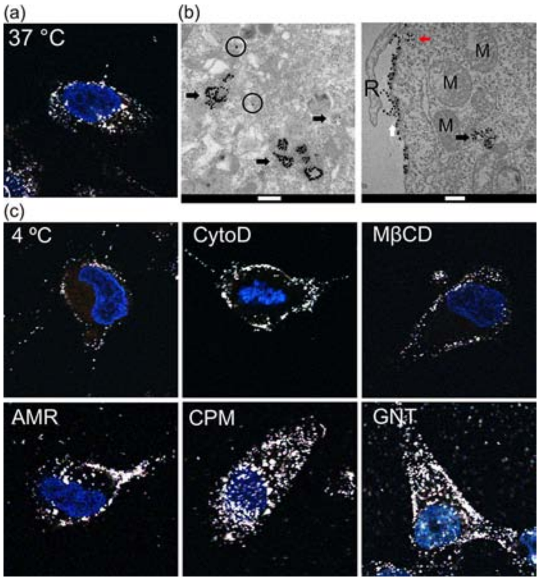

Figure 2. TAT-NS cellular uptake. (a) TPL image of TAT-NS incubated with BT549 cells for 1 h at 37 °C without inhibitors. (b) TEM images of TAT-NS in vesicles (black arrows), cytoplasm (circles), membrane (white arrow), and upon invagination (red arrow). R, ruffle; M, mitochondria; scale bar, 500 nm. (c) TPL images of TAT-NS-treated cells under different inhibitors. Cellular uptake of TAT-NS was inhibited by 4 °C, cytoD, MβCD, and AMR but not CPM and GNT. Nuclei are stained blue. TPL images size, 50×50 μm^2.

endocytosis. In agreement with Kreptic et al. and Berry et al., some particles are observed outside the vesicles in the cytoplasm;[14a,b] this may reflect particles leaking out from macropinosomes into the cytoplasm. All these features are in concordance to the behavior of macropinocytosis.

To further assess the TAT-NS internalization pathway, cells were pretreated with several inhibitors for 30 min, incubated with TAT-NS for 1 h, then examined under TPL microscopy (Figure 2c) following a previous protocol.[18] We found that TAT-NS internalization was inhibited by 4 °C (energy blockade), amiloride (AMR; lowering sub-membraneous pH), cytochalasin D (cytoD; F-actin inhibition), and methyl-β-cyclodextrin (MβCD; lipid raft inhibition), but not chlorpromazine (CPM; clathrin inhibition), genistein (GNT; caveola inhibition), or nocodazole (NCZ; microtubule disruption; data not shown). This confirms that TAT-NS internalization is an energy-dependent, actin-driven, and lipid raft-mediated macropinocytosisy.[13] Clathrin or caveola, although previously reported to facilitate TAT uptake,[10a] may play a less significant role in this cell type. TAT-NS adhesion to the plasma membrane and actin ruffles, however, were not inhibited because the multidentate hydrogen bonding is not affected by the inhibitors. Based on the TEM/TPL results and inhibitor studies, we believe that the primary TAT-NS uptake pathway is through actin-driven and lipid raft-mediated macropinocytosis.

Before the photothermolysis study, we need to ensure sufficient intracellular TAT-NS delivery without compromising cell viability, so we examined the temporal uptake profile along with the cytotoxicity assay. Figure 3a shows the time-dependent uptake of TAT-NS on BT549 cells. In 10 min, TAT-NS started anchoring onto the plasma membrane. Real-time live cell TPL imaging confirmed surface binding by showing single free-moving TAT-NS adhering inhomogeneously to the surface membrane (Video S1). Within 1 h, intracellular uptake can be seen, forming larger-sized punctates on TPL images. These large, bright punctates, ~1 μm by TPL microscopy, were most likely macropinosomes. Smaller and dimmer punctates might be smaller vesicles or even single NS. Later, TAT-NS accumulated toward the perinuclear region and eventually "saturated" the cytoplasm, with numerous large, bright punctates at 24 h. Under TEM , these large, bright punctates in the TPL images were seen to be mostly TAT-NS accumulated in vesicles (Figure S3). Krpetic et al. also observed particle accumulation, mostly in the vesicles at 24 h, but particles were cleared after replacing the growth medium.[14a] The fate of TAT-NS after 24 h was not examined in this study. It is possible that macropinosomes interact little with endosomal compartments and recycle their contents back to the extracellular space,[10a,14a] but a detail discussion is beyond the scope of this article.

Figure 3b illustrates that cellular metabolic activity was affected by TAT-NS after 24-h incubation, depending on both the coating type (bare, PEG, TAT) and particle concentration (Figure 3c). At 8-h incubation, cell viability is not significantly different from the control (0 h), but the statistical distribution of viability is wide. Although a higher particle density under longer incubation is desired for higher photothermolysis efficiency, to reduce the confounding effect from altered cell viability we chose 4-h TAT-NS incubation for the photothermolysis study.

Photothermolysis was performed on the same multiphoton microscope with raster scanning for 3 min (Figure 3d). Average irradiance (i.e., the power density) was controlled by the acoustic-optic modulator and the scanning area from the microscope's software. At 1 mW (12.5 pJ/pulse; 0.4 W/cm^2 irradiance), no laser-induced damage was seen on cells treated 4 h with media only or PEG-NS. Irradiation also did not damage cells immersed in PEG-NS (0.1 nM) (data not shown), most likely because the free-floating PEG-NS were not concentrated enough in cells. In contrast, a distinct square of ablation (empty area) was observed when irradiating (0.4 W/cm^2) cells incubated 4 h with TAT-NS. Real-time live cell TPL imaging showed cells shrinking or moving outward upon irradiation (Video S2). At 0.5 mW (6.25 pJ/pulse; 0.2 W/cm^2 irradiance), a large portion of cells were damaged (showing red) but still attached on the dish. This irradiance is not only lower than previously reported values using a pulsed laser[6a,9a] but also lower than the MPE of skin to laser irradiation (0.4 W/cm^2 at 850 nm) per ANSI regulation.[8] This is the first demonstration of cellular photothermal therapy at such a low irradiance. With longer incubation time (more NS inside cells), the required irradiance could be even lower (Figure S4). Combination of pulsed laser irradiation and enhanced intracellular delivery of TAT-NS clearly makes a very efficient photothermolysis system.

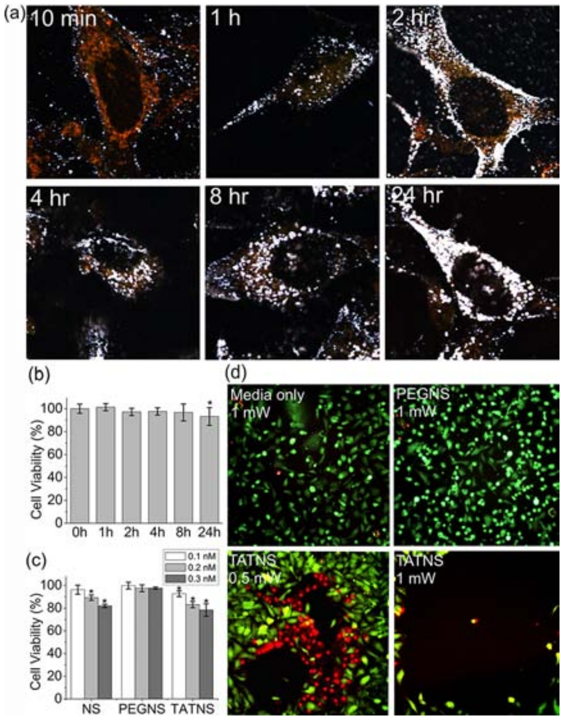

Figure 3. (a) Time series TPL images of TAT-NS-treated cells (white) showing incremental accumulation. Cytoplasm is stained orange. Image size, 50×50 μm^2. (b) Time series viability on cells incubated with TAT-NS up to 24 h. (c) Cell viability at 24 h on NS of different surface coatings (bare, PEG, TAT) and concentrations (0.1–0.3 nM). *$p < 0.05$. (d) Photothermolysis (850 nm, 0.5 or 1 mW, scanning area 500×500 μm^2, 3 min) on BT549 cells incubated 4 h with media only, PEG-NS, and TAT-NS. Live/dead cells are green/red. Image size, 612×612 μm^2.

Note that our TAT-NS, with TAT and PEG coating, exhibit beneficial properties of each. For *in vitro* study, PEGylation prevents cellular uptake of NP, hence requiring addition of TAT. For *in vivo* study, the task is even more challenging, requiring consideration of, e.g., circulating half-life, reticuloendothelial system clearance, vascular permeation, and active targeting.[1a,d,19] PEGylation extends the NP's circulation half-life and hence promotes passive accumulation of NP in the area of enhanced vascular permeability (e.g., large tumors). For regions with normal vascular permeability or even limited permeability (e.g., small tumors), PEGylation may not be sufficient. That may explain why in some cases intra-tumoral injection is preferred for photothermal therapy.[19c] As described earlier, TAT functionalization may facilitate the crossing of the BBB,[12d,e] which usually blocks the permeation of many chemicals and NP. Whether TAT-NS facilitate the accumulation of NP in brain tumors remains to be studied. Such discussion is beyond the scope of this paper.

Our results demonstrate efficient photothermolysis at an ultralow irradiance ($0.2\ \mathrm{W/cm^2}$), which is the lowest value ever reported for pulsed laser powers. The enhanced intracellular delivery of TAT-NS substantially potentiates the photothermolysis efficiency without compromising cell viability. The traceability of NS by multiphoton microscopy greatly simplifies both the study of the particles' intracellular trafficking and the monitoring of the photothermolysis process on live cells. Since multiphoton microscopes utilize tissue-penetrating NIR lasers, photothermolysis on deep-seated tumors is possible. Combining NS and TPL microscopy also makes it possible to gain a mechanistic understanding of the particles' kinetic behavior. Uptake of TAT-NS examined by both TEM and multiphoton microscopy confirms that the uptake mechanism involves primarily actin-driven lipid raft-mediated macropinocytosis. Future research would extend this work to selective delivery of cargo to target tissues (e.g., tumors). With further development, gold nanostars can be promising theranostic agents in cancer therapy.

■ ASSOCIATED CONTENT

Ⓢ Supporting Information

Procedures, figures, and videos. This material is available free of charge via the Internet at http://pubs.acs.org.

■ AUTHOR INFORMATION

Corresponding Author

tuan.vodinh@duke.edu

Notes

The authors declare no competing financial interest.

■ ACKNOWLEDGMENTS

This work was sponsored by the Duke University Faculty Research Funds, the National Institutes of Health (Grant R01 EB006201), and Immunolight, LLC. A.M.F. is supported by an NIH training grant (T32 EB001040).

■ REFERENCES

(1) (a) Kievit, F. M.; Zhang, M. *Adv. Mater.* **2011**, *23*, H217. (b) Shi, J.; Votruba, A. R.; Farokhzad, O. C.; Langer, R. *Nano Lett.* **2010**, *10*, 3223. (c) Chadwick, S.; Kriegel, C.; Amiji, M. *Adv. Drug Delivery Rev.* **2010**, *62*, 394. (d) Riehemann, K.; Schneider, S. W.; Luger, T. A.; Godin, B.; Ferrari, M.; Fuchs, H. *Angew. Chem., Int. Ed.* **2009**, *48*, 872. (e) Wang, X.; Yang, L.; Chen, Z. G.; Shin, D. M. *CA Cancer J. Clin.* **2008**, *58*, 97.

(2) (a) Hahn, M. A.; Singh, A. K.; Sharma, P.; Brown, S. C.; Moudgil, B. M. *Anal. Bioanal. Chem.* **2011**, *399*, 3. (b) Ghosh, P.; Han, G.; De, M.; Kim, C. K.; Rotello, V. M. *Adv. Drug Delivery Rev.* **2008**, *60*, 1307. (c) Juzenas, P.; Chen, W.; Sun, Y.-P.; Neto Coelho, M. A.; Generalov, R.; Generalova, N.; Christensen, I. L. *Adv. Drug Delivery Rev.* **2008**, *60*, 1600. (d) Kennedy, L. C.; Bickford, L. R.; Lewinski, N. A.; Coughlin, A. J.; Hu, Y.; Day, E. S.; West, J. L.; Drezek, R. A. *Small* **2011**, *7*, 169.

(3) (a) Hu, M.; Chen, J.; Li, Z.-Y.; Au, L.; Hartland, G. V.; Li, X.; Marquez, M.; Xia, Y. *Chem. Soc. Rev.* **2006**, *35*, 1084. (b) Boisselier, E.; Astruc, D. *Chem. Soc. Rev.* **2009**, *38*, 1759.

(4) (a) Guerrero-Martínez, A.; Barbosa, S.; Pastoriza-Santos, I.; Liz-Marzán, L. M. *Curr. Opin. Colloid Interface Sci.* **2011**, *16*, 118. (b) Yuan, H.; Khoury, C. G.; "co-first author"; Hwang, H.; Wilson, C. M.; Grant, G. A.; Vo-Dinh, T. *Nanotechnology* **2012**, *23*, 075102. (c) Yuan, H.; Khoury, C. G.; Wilson, C. M.; Grant, G. A.; Bennett, A. J.; Vo-Dinh, T. *Nanomedicine: NBM* **2012**, DOI: 10.1016/j.nano.2012.02.005.

(5) (a) Austin, L. A.; Kang, B.; Yen, C.-W.; El-Sayed, M. A. *J. Am. Chem. Soc.* **2011**, *133*, 17594. (b) Tkachenko, A. G.; Xie, H.; Liu, Y.; Coleman, D.; Ryan, J.; Glomm, W. R.; Shipton, M. K.; Franzen, S.; Feldheim, D. L. *Bioconjugate Chem.* **2004**, *15*, 482.

(6) (a) Tong, L.; Wei, Q.; Wei, A.; Cheng, J.-X. *Photochem. Photobiol.* **2009**, *85*, 21. (b) Hutter, E.; Maysinger, D. *Microsc. Res. Tech.* **2010**, *74*, 592.

(7) (a) Van de Broek, B.; Devoogdt, N.; D'Hollander, A.; Gijs, H.-L.; Jans, K.; Lagae, L.; Muyldermans, S.; Maes, G.; Borghs, G. *ACS Nano* **2011**, *5*, 4319. (b) Baffou, G.; Quidant, R.; Girard, C. *Appl. Phys. Lett.* **2009**, *94*, 153109.

(8) ANSI. *American National Standard for safe use of lasers*; Laser Institute of America: Orlando, FL, 2000.

(9) (a) Au, L.; Zheng, D.; Zhou, F.; Li, Z.-Y.; Li, X.; Xia, Y. *ACS Nano* **2008**, *2*, 1645. (b) Kim, J.; Park, S.; Lee, J. E.; Jin, S. M.; Lee, J. H.; Lee, I. S.; Yang, I.; Kim, J.-S.; Kim, S. K.; Cho, M.-H.; Hyeon, T. *Angew. Chem., Int. Ed.* **2006**, *45*, 7754.

(10) (a) Patel, L.; Zaro, J.; Shen, W.-C. *Pharm. Res.* **2007**, *24*, 1977. (b) Khalil, I. A.; Kogure, K.; Akita, H.; Harashima, H. *Pharmacol. Rev.* **2006**, *58*, 32.

(11) (a) Lévy, R.; Shaheen, U.; Cesbron, Y. *Nano Rev.* **2010**, *1*, 4889. (b) Lundqvist, M.; Stigler, J.; Elia, G.; Lynch, I.; Cedervall, T.; Dawson, K. A. *Proc. Natl. Acad. Sci. U.S.A.* **2008**, *105*, 14265. (c) Bartczak, D.; Muskens, O. L.; Nitti, S.; Sanchez-Elsner, T.; Millar, T. M.; Kanaras, A. G. *Small* **2012**, *8*, 122.

(12) (a) Torchilin, V. P. *Adv. Drug Delivery Rev.* **2008**, *60*, 548. (b) Wei, Y.; Jana, N. R.; Tan, S. J.; Ying, J. Y. *Bioconjugate Chem.* **2009**, *20*, 1752. (c) Zhao, M.; Kircher, M. F.; Josephson, L.; Weissleder, R. *Bioconjugate Chem.* **2002**, *13*, 840. (d) Rao, K. S.; Reddy, M. K.; Horning, J. L.; Labhasetwar, V. *Biomaterials* **2008**, *29*, 4429. (e) Tian, X.-h.; Wei, F.; Wang, T.-x.; Wang, D.; Wang, J.; Lin, X.-n.; Wang, P.; Ren, L. *Mater. Lett.* **2012**, *68*, 94.

(13) (a) Wadia, J. S.; Stan, R. V.; Dowdy, S. F. *Nat. Med.* **2004**, *10*, 310. (b) Ruan, G.; Agrawal, A.; Marcus, A. I.; Nie, S. *J. Am. Chem. Soc.* **2007**, *129*, 14759.

(14) (a) Krpetic, Z.; Saleemi, S.; Prior, I. A.; Sée, V.; Qureshi, R.; Brust, M. *ACS Nano* **2011**, *5*, 5195. (b) Berry, C. C.; de la Fuente, J. M.; Mullin, M.; Chu, S. W. L.; Curtis, A. S. G. *IEEE Trans. Nanobiosci.* **2007**, *6*, 262.

(15) Durr, N. J.; Weisspfennig, C. T.; Holfeld, B. A.; Ben-Yakar, A. *J. Biomed. Opt.* **2011**, *16*, 026008.

(16) (a) Pan, L.; He, Q.; Liu, J.; Chen, Y.; Ma, M.; Zhang, L.; Shi, J. *J. Am. Chem. Soc.* **2012**, *134*, 5722. (b) Panté, N.; Kann, M. *Mol. Biol. Cell* **2002**, *13*, 425.

(17) Mishra, A.; Lai, G. H.; Schmidt, N. W.; Sun, V. Z.; Rodriguez, A. R.; Tong, R.; Tang, L.; Cheng, J.; Deming, T. J.; Kamei, D. T.; Wong, G. C. L. *Proc. Natl. Acad. Sci. U.S.A.* **2011**, *108*, 16883.

(18) (a) Zhang, L. W.; Monteiro-Riviere, N. A. *Toxicol. Sci.* **2009**, *110*, 138. (b) Iversen, T.-G.; Skotland, T.; Sandvig, K. *Nano Today* **2011**, *6*, 176.

(19) (a) Lal, S.; Clare, S.; Halas, N. J. *Acc. Chem. Res.* **2008**, *41*, 1842. (b) Fang, J.; Nakamura, H.; Maeda, H. *Adv. Drug Delivery Rev.* **2011**, *63*, 136. (c) Huang, X.; Peng, X.; Wang, Y.; Wang, Y.; Shin, D. M.; El-Sayed, M. A.; Nie, S. *ACS Nano* **2010**, *4*, 5887.